Time-Resolved Resonance Raman Study on the Binding of Carbon Monoxide to Recombinant Human Myoglobin and Its Distal Histidine Mutants†

Yoshinao Sakan, Takashi Ogura, and Teizo Kitagawa*

Institute for Molecular Science, Okazaki National Research Institutes and the Graduate University for Advanced Studies, Myodaiji, Okazaki, 444 Japan

Frank A. Fraunfelter, Rafael Mattera, and Masao Ikeda-Saito

Department of Physiology and Biophysics, Case Western Reserve University School of Medicine, Cleveland, Ohio 44106-4079

Received January 13, 1993

ABSTRACT: Time-resolved resonance Raman (RR) spectra of the recombined species of photodissociated CO with recombinant human myoglobin (Mb) and several E7 mutants, in which distal His was replaced by Gly (H64G), Gln (H64Q), Ala (H64A), Ile (H64I), Val (H64V), and Leu (H64L) through site-directed mutagenesis, were observed in the time range −20 ns to 1 ms following photolysis. The Fe–CO stretching (ν_{Fe-CO}) RR band was observed successfully with pulse excitation when the laser power was greatly reduced. H64H, H64G, and H64Q gave the ν_{Fe-CO} band at 505–510 cm^{-1} in their stationary states. In their recovery processes 1–100 μs after photodissociation, a broad transient band was observed at slightly lower frequencies than those of their equilibrium structures for H64G and H64Q, but a transient ν_{Fe-CO} band corresponding to the so-called "open" form was not identified around 490 cm^{-1} for any of the three species. A second group, H64A, H64I, H64V, and H64L, gave the main ν_{Fe-CO} band at 490–495 cm^{-1} with a shoulder around 510 cm^{-1} (except for H64L) in the stationary state and exhibited a much faster recovery than the first group. These latter four species gave a broad transient band around 492–500 cm^{-1} in the time range of 100–1000 ns, while the ~510 cm^{-1} shoulder appeared much later. The equilibrium relative intensity of the two bands was attained at 500 μs, suggesting that the interconversion between the two forms is slower than 100 μs. For all MbCO examined here, the recovery, determined from the area intensity of the ν_{Fe-CO} band, exhibited two phases irrespective of the presence of one or two ν_{Fe-CO} bands. The ν_{Fe-CO} frequencies could be correlated with the hydropathy index of the E7 residue but not with its physical size. It is inferred that the more hydrophobic environment around CO reduces the polarization of CO and lowers the ν_{Fe-CO} frequency to ~490 cm^{-1} on the one hand and stabilizes the intermediate state called the protein-separated pair on the other. The latter increases the contribution of recombination from this intermediate, resulting in faster recombination of CO.

Molecular structures of myoglobin (Mb), an oxygen storage protein, and its CO complex (MbCO)[1] have been determined by X-ray crystallography at a level of 1.5-Å resolution, and it has been noted that there is no pathway for the migration of a ligand from solvent to the buried binding site in the heme pocket (Kuriyan et al., 1986). It is of fundamental importance in the study of the structure–function relationships of these proteins to elucidate the rapid rearrangements of the globin structure accompanying the ligand entry. While the O_2 complex of Mb (MbO_2) adopts a "closed" structure (Phillips, 1980) similar to MbCO, X-ray studies of the ethyl isocyanide complex ($MbCNC_2H_5$) reveal the opening of a pathway for ligand entry (Johnson et al., 1989), presumably due to steric repulsion between the bulky ethyl group and distal residues; accordingly, its structure has been regarded as the model of an "open" form. Champion and co-workers (Morikis et al., 1989; Sage et al., 1991) have investigated the pH-dependent change of the open/closed equilibrium, but there has been no direct time-resolved measurement for the protein structural change upon ligand entry.

Photodissociation of CO from Mb and hemoglobin (Hb) has been extensively investigated in attempts to understand the dynamical features of proteins (Hofrichter et al., 1983; Henry et al., 1983; Martin et al., 1983; Braunstein et al., 1988; Moore et al., 1988; Patrich et al., 1988; Anfinrud et al., 1989; Rohlfs et al., 1990; Carver et al., 1990; Srajer et al., 1991; Traylor et al., 1992; Tian et al., 1992). Photodissociation of MbCO followed by relaxation to the stable high-spin heme is reported to take place in 350 fs (Martin et al., 1983). IR studies on the CO stretching (ν_{CO}) mode indicated that 85% of photodissociated CO remains in the globin 1 ns after photolysis and 50% remains after 50 ns (Anfinrud et al., 1989), although there is no return of CO to the heme in the 200–8000-ps range (Traylor et al., 1992). The visible absorption spectrum of the photolysis product of MbCO is reported to be the same as that of the equilibrium deoxyMb for all times greater than 3 ns (Henry et al., 1983), although a recent transient absorption study (Tian et al., 1992) revealed that the geminate recombination of photodissociated CO was nonexponential and, thus, that the distal pocket relaxation might be nonequilibrium. However, the bimolecular process in the 10 μs to 1 ms range is expected to reflect the thermal binding.

† This study was supported by a Grant-in-Aid from the Ministry of Education, Science, and Culture, Japan, for Priority Areas (Bioinorganic Chemistry, 03241105) (T.K.), by an NIH BRGS grant (RR05410-28) (R.M.), by NIH research grants (GM39492 and GM39359) (M.I.-S.), and a grant-in-aid from the Northeast Ohio Affiliate of the American Heart Association (M.I.-S.).

* Author to whom correspondence should be addressed.

[1] Abbreviations: MbCO, carbon monoxide adduct of myoglobin; HbCO, carbon monoxide adduct of hemoglobin; RR, resonance Raman.

0006-2960/93/0432-5815$04.00/0

In most of these kinetic studies transient absorption spectroscopy was used, which did not allow for a detailed discussion of the molecular structure. In contrast, resonance Raman (RR) spectroscopy, which reveals a vibrational spectrum of the protein chromophore, is capable of providing detailed structural information (Kitagawa, 1986; Spiro, 1989). The Fe–CO stretching (ν_{Fe-CO}) frequency of the heme–CO complexes is known to be sensitive to the CO geometry in the heme pocket (Yu et al., 1983; Yu & Kerr, 1988; Li & Spiro, 1988; Nagai et al., 1991), and the differences in the ν_{Fe-CO} frequency between heme proteins and model heme–CO complexes are ascribed to tilting or bending of the Fe–C–O linkage in the protein (Yu et al., 1983; Yu & Kerr, 1988). The ν_{Fe-CO} frequencies are known to have a linear inverse correlation with the ν_{CO} frequencies (Tsubaki et al., 1982; Yu et al., 1983; Yu & Kerr, 1988; Li & Spiro, 1988). From ab initio MO calculations, Augspurger et al. (1991) have also demonstrated that the ν_{CO} frequency is correlated with the ^{13}C NMR shift of the ^{13}CO ligand and is affected by the electric field at the CO ligand, which for MbCO is generated by the surrounding amino acid residues and would cause an electronic polarization of the C–O bond. Whatever the origin, the ν_{Fe-CO} frequency is expected to reflect the protein structure around the CO ligand.

On the other hand, a role of the highly conserved distal histidine (E7-His or His-64), which forms a hydrogen bond to bound O_2 to stabilize the oxy form (Yonetani et al., 1974; Phillips & Shoenborn, 1981; Kitagawa et al., 1982) and is deduced to destabilize the CO form through steric hindrance (Collman et al., 1983), has been a matter of physicochemical concern. Recent kinetic studies suggested that CO entered into the binding site through a channel between the E7-His and distal valine (Val-68) (Rohlfs et al., 1990), and therefore the orientation of the side chain of E7-His, whose mobility depends on the position of the Arg-45 side chain, would determine the opening/closing of the gate for ligand entry (Kuriyan et al., 1986) as well as the equilibrium CO–heme geometry (Collman et al., 1983). In fact, the ν_{Fe-CO} frequency was reported to be altered by replacement of distal His for sperm whale Mb (Morikis et al., 1989) and human Hb (Lin et al., 1990). The X-ray study (Kuriyan et al., 1986) demonstrated the positional uncertainty only for the Arg-45 of sperm whale MbCO (two positions with 50% occupancy). The abnormal subunit of M-type Hbs, in which E7-His is replaced by Tyr, gave the ν_{Fe-CO} RR band at a distinctly lower frequency ($\sim$490 cm^{-1}), and the heme–CO was apparently not photodissociated by the weak laser illumination known to dissociate the normal subunit (Nagai et al., 1991).

The ν_{Fe-CO} RR band of acidified sperm whale MbCO was also found at a lower frequency (488–489 cm^{-1}) (Morikis et al., 1989; Ramsden & Spiro, 1989; Han et al., 1990; Zhu et al., 1992) than that of neutral MbCO (507 cm^{-1}), and the low-frequency shift was ascribed to a structural change of the CO–heme to an upright geometry following the swinging out of the His-64 side chain from the heme pocket upon its protonation, thus removing the steric hindrance to CO (Ramsden & Spiro, 1989; Zhu et al., 1992). This conformational change of His-64 results in the opening of a pathway for ligand entry, and accordingly, the two ν_{Fe-CO} frequencies of the neutral (507 cm^{-1}) and acidic MbCO ($\sim$488 cm^{-1}) were considered to represent the closed and open forms of the heme pocket (Morikis et al., 1989; Sage et al., 1991; Zhu et al., 1992).

If CO binds to the heme in the so-called open form and relaxes to the closed form at neutral pH, and this relaxation is relatively slow as seen for MbCO crystals and frozen solutions (Zhu et al., 1992), the ν_{Fe-CO} RR band is expected to exhibit a temporal shift from 488 to 507 cm^{-1} during the recombination process of the photodissociated CO. In fact, for acidified horse MbCO, two ν_{Fe-CO} RR bands were resolved for transient species and their recovery rates appeared distinctly different (Sakan et al., 1992). In some mutant MbCOs, the corresponding two structures may be in an equilibrium at neutral pH, and if the interconversion between the two structures is sufficiently fast in contrast with the acidified horse MbCO, the two bands are expected to grow simultaneously with the intensity ratio of the equilibrium state. When a mutant has a predominantly upright geometry corresponding to the open form, the structural relaxation would be unnecessary and consequently recombination of CO would be fast.

To examine the validity of the open/closed model from these points of view, time-resolved resonance Raman (TR^3) experiments were carried out for recombinant human MbCO and several E7 mutants, in which distal His was replaced by Gly (H64G), Gln (H64Q), Ala (H64A), Ile (H64I), Val (H64V), and Leu (H64L) through site-directed mutagenesis. Our results indicate that the mutants with ν_{Fe-CO} around 490 cm^{-1} generally recover faster than those with ν_{Fe-CO} around 507 cm^{-1}. Although this is apparently consistent with the assignments of the $\sim$490 and $\sim$507 cm^{-1} bands to the open and closed forms, respectively, the ν_{Fe-CO} frequency becomes lower as the E64 residue becomes more hydrophobic, unrelated to the bulkiness of its side chain. We also note that, for the mutants with ν_{Fe-CO} around 507 cm^{-1}, the $\sim$490 cm^{-1} band does not appear before the appearance of the $\sim$507 cm^{-1} band and that the transient state around 500 ns after photolysis under 1 atm of CO is not always the same as the equilibrium state, whether of the $\sim$490 or $\sim$507 cm^{-1} type. These results are in agreement with those from our previous TR^3 studies on neutral and acidified horse MbCO (Sakan et al., 1992).

EXPERIMENTAL PROCEDURES

The human Mb expression system (Varadarajan et al., 1985) was a kind gift from Dr. S. G. Boxer of Stanford University. The induction of fusion proteins in AR68 and purification of Mb were carried out as reported by Varadarajan et al. (1989) and Ikeda-Saito et al. (1992). The reference protein used here, H64H, was originally designated as C110A (Varadarajan et al., 1989), in which Cys-110 was replaced by Ala for ease of purification. The spectroscopic and functional properties of this mutant were indistinguishable from those of the wild-type Mb (Varadarajan et al., 1989), and therefore we designate C110A as the wild-type (H64H). All of the mutant recombinant Mbs gave a single band electrophoretically, and their NMR spectra in the met-form confirmed that there is no disorder of hemes (upside down, etc.).

Time-resolved RR spectra were obtained with two 10-ns pulsed lasers operating at 10 Hz. The probe beam (416 nm) was generated by the H_2–first Stokes shift of the third harmonic of an Nd:YAG laser (Quanta-Ray, DCR-3), and its power was made as low as possible (100-125 μJ/pulse at the sample) to avoid the spectral appearance of photodissociated species. The pump beam (532.0 nm) was the second harmonic of an Nd:YAG laser (Quanta-Ray, GCR-11), and its power was adjusted to 4.4 mJ/pulse at the sample. The pump and probe beams were made strictly collinear by a dichroic mirror, and the superimposed beams were line-focused onto the sample by two cylindrical lenses. The delay time (Δt_d) between the probe pulse and the pump pulse was controlled for settings between −20 ns and 1 ms through the independent firing of

each laser's Q switches by a pulse generator (Stanford Research, DG-535) and was monitored on an oscilloscope (Tektronix 2445B) by photodiode detection (Hamamatsu, S1722-02). The uncertainty in Δt_d was ±2 ns. Spectra were recorded for delay times of Δt_d = −20, 0, 20, 100, and 500 ns, 1, 10, 100, and 500 μs, and 1 ms, in that order, and for each sample under the same instrumental conditions. After the last measurement (Δt_d = 1 ms), the appearance of the first spectrum (Δt_d = −20 ns) was always confirmed.

Scattered light at right angles was collected and focused by two synthetic quartz lenses onto an entrance slit of a triple polychromator (Spex 1877) equipped with a nonblazed holographic grating (Milton-Roy, 2400 grooves/mm) and an intensified photodiode array (PAR, OMA-III 1421B). The data for each spectrum were accumulated for ca. 70 min on an OMA III system and then transferred to a personal computer (NEC PC-9801DA) for further analysis. The whole series of experiments was carried out twice for independent preparations of mutant Mbs, and thus the reproducibility of the present results could be confirmed.

About 1.5 mL of 25 μM ferric Mb solution (50 mM Tris-HCl buffer at pH 8.0) was transferred to an airtight spinning cell (diameter = 20 mm), into which CO gas was incorporated to a pressure of 1 atm (after evacuation of the internal pressure to 0.01 mmHg). The pump/fill procedure was repeated at least three times, and finally, for reduction of ferric Mb and complete removal of oxygen, a small amount of degassed dithionite solution was added so that the final concentration was 10 mM. At this concentration, nonresonant Raman bands of dithionite around 460 and 580 cm^{-1} do not disturb the RR spectra of MbCO. The cell was rotated slowly (25 rpm) in order to avoid two successive probe pulses irradiating the same sample volume and also to allow for the recombination of Mb and CO from the photodissociated state in one turn (2.4 s) of the spinning cell. This corresponds to a flow rate for the sample of 26 μm/ms. Since the laser spot sizes of the probe and pump beams are 100 and 200 μm, respectively, the pump-illuminated volume still stays in the probe-illuminated volume, even at 1 ms after the photolysis, but is replaced with a fresh one before the next probe pulse comes (100 ms). Cold N_2 gas was flushed against the spinning cell to maintain it at 10 °C. The Raman shifts were calibrated with indene and CCl_4 and determined with an accuracy of ±1 cm^{-1} for well-defined peaks.

The integrated intensity of a Raman band was obtained with either of two methods after the assumption of a linear base line between both ends of integration, an example of which is the broken line in the spectrum of H64H (Figure 2). One method is a computer summation of the areas of individual channels within the band. In this case the spike noise may affect the results. The second method is to weigh the cut papers of the smoothed spectra. In the latter case, the intensity was determined to be an average of 10 cut papers. The two methods qualitatively yielded the same results. Band-fitting calculations were carried out with Lorentzian functions by using the damped least-squares method (Levenberg, 1944; Senga & Minami, 1986).

RESULTS

Static Spectra. The RR spectra of the mutant deoxyMbs in the 1200-1700 cm^{-1} region (not shown) were similar to those of native deoxyMb. Figure 1 shows the stationary-state RR spectra in the ν_{Fe-CO} region of the seven MbCO species observed without the pump beam. These spectra are in agreement with those observed with a high-speed (1800 rpm) spinning cell and CW laser excitation at 406.7 nm. Although

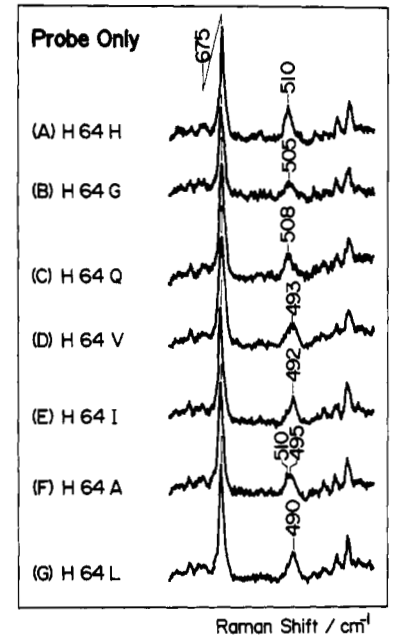

FIGURE 1: Probe-only RR spectra in the ν_{Fe-CO} region of the wild-type human MbCO (H64H) and its E7-Gly (H64G), E7-Gln (H64Q), E7-Val (H64V), E7-Ile (H64I), E7-Ala (H64A), and E7-Leu (H64L) mutants. Experimental conditions: sample concentration, 25 μM; excitation, 416 nm, 100–125 μJ/pulse; exposure time, 8 s; number of scans, 500.

there may be an appreciable amount of photodissociated species present, Figure 1 demonstrates that the remaining CO-bound form can be monitored by pulse excitation when the laser power is greatly reduced.

The maximum intensity of the ν_{Fe-CO} band is seen at 510–505 cm^{-1} for H64H, H64G, and H64Q and at 495–490 cm^{-1} for H64V, H64I, H64A, and H64L, while the porphyrin ν_7 mode (the mode number is based on Abe et al. (1978)) remains unshifted at 675 ± 1 cm^{-1} (only H64G gives it at 677 cm^{-1}) by E7 mutation. The assignment of the ν_{Fe-CO} band was confirmed by the observation of isotopic frequency shifts for $^{13}C^{16}O$ (−4 cm^{-1} for H64Q and −4.5 cm^{-1} for H64L). The Fe–C–O bending band was too weak to be identified for all of the samples. H64H and H64L seem to yield a single ν_{Fe-CO} band but others give unresolved multiple bands. On the basis of the main ν_{Fe-CO} frequencies, H64H (510 cm^{-1}), H64G (505 cm^{-1}), and H64Q (508 cm^{-1}) are of the normal type, but H64V (493 cm^{-1}), H64I (492 cm^{-1}), H64A (495 cm^{-1}), and H64L (490 cm^{-1}) are of the acidified MbCO type (Morikis et al., 1989; Sage et al., 1991; Ramsden & Spiro, 1989; Han et al., 1990; Zhu et al., 1992; Sakan et al., 1992) or distal His mutant HbMCO type (Nagai et al., 1991). It is apparent that the ν_{Fe-CO} frequencies cannot be classified solely on bulkiness of the E7 residue, as first pointed out by Nagai et al. (1987).

Time-Resolved RR Spectra of H64H, H64G, and H64Q. The TR³ spectra for H64H and H64G are displayed in Figures 2 and 3, respectively. The ordinate scales of spectra A–F in each figure are common. Since the instrumental conditions, including the laser power, the exposure time of the diode array detector, and the accumulation time, are the same for all measurements except for variation of Δt_d, the intensity of the Raman bands delineated in the figures reflects the real populations of MbCO present at each Δt_d, although we failed to incorporate an internal intensity standard (sodium cacodylate as an intensity standard photoreacted with dithionite during the measurements). The spectra for Δt_d = −20 ns, which correspond to the pump/probe spectra for a delay time,

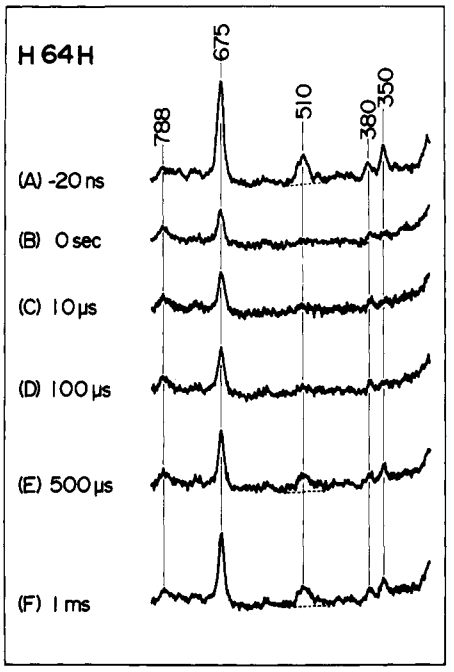

FIGURE 2: Pump/probe RR spectra in the ν_{Fe-CO} region of wild-type human MbCO. The delay time of the probe beam from the pump beam is specified at the left side of each spectrum (to ±2 ns). Broken lines indicate the assumed base lines. Instrumental conditions: probe beam, 416 nm, 100–125 μJ/pulse; pump beam, 532 nm, 4.4 mJ/pulse; exposure time, 8 s; number of scans, 500.

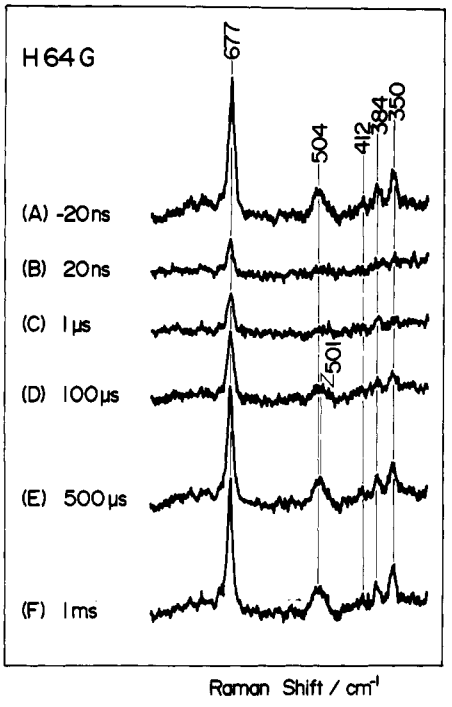

FIGURE 3: Pump/probe RR spectra in the ν_{Fe-CO} region of the E7-Gly mutant MbCO. Experimental conditions are the same as those for Figure 2.

Δt_d = 2.4 s, equal to the period for one turn of the spinning cell, are in agreement with the spectra observed without the pump beam (Figure 1). This indicates that recombination of CO to photodissociated species is completed in one turn of the spinning cell. Disappearance of the ν_{Fe-CO} band for Δt_d = 0 ns means that photodissociation is achieved by the pump beam. Since the excitation wavelength (416 nm) is closer to the Soret maximum of MbCO (424 nm) than to that of deoxyMb (435 nm), the RR spectrum of the CO-bound form is expected to be more enhanced than that of deoxyMb.

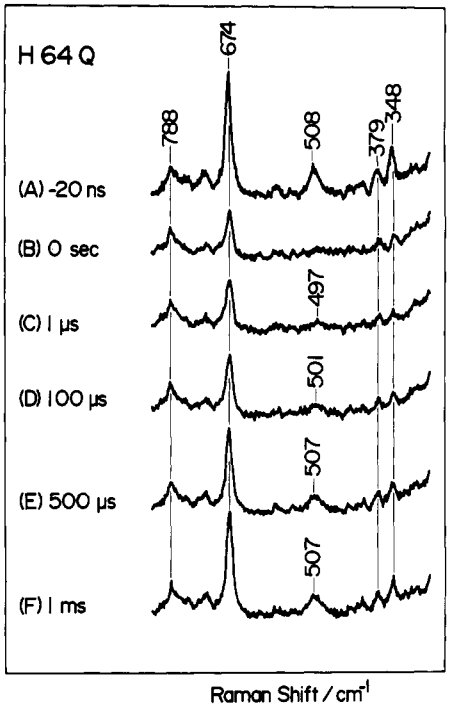

FIGURE 4: Pump/probe RR spectra in the ν_{Fe-CO} region of the E7-Gln mutant MbCO. Experimental conditions are the same as those for Figure 2.

The ν_{Fe-CO} band of H64H at 510 cm^{-1} starts to increase in intensity from 100 μs, but it has still not fully recovered at Δt_d = 1 ms. The band shapes at 500 μs and 1 ms are similar, and it is difficult to assume the presence of a transient band around 490 cm^{-1} in the spectra for Δt_d = 10–500 μs. For H64G the ν_{Fe-CO} band is discernible in an earlier time range (Δt_d = 1–100 μs), despite the fact that the equilibrium ν_{Fe-CO} frequency is higher than 500 cm^{-1}. The center of the transient band is shifted slightly to a lower frequency and its band width is broader. If the 490 cm^{-1} species were present and the conversion from the open to closed form were slow, the 490 cm^{-1} band should have been observed separately in the present spectral resolution, as was confirmed for acidified horse MbCO (Sakan et al., 1992). This means that a species present at Δt_d = 1–100 μs is different from the 490 cm^{-1} species. The band center returns to the original position at Δt_d = 1 ms.

A similar but more conspicuous feature was observed for H64Q, as shown in Figure 4. The TR^3 spectra for Δt_d = 1 (C) and 100 μs (D) give rise to a weak and a broad band at 497 and 501 cm^{-1}, respectively, but their frequencies are not as low as the 490 cm^{-1} expected for the open form. The transient band with heterogeneous broadening gradually returns to the original position (508 cm^{-1}) as the recombination proceeds, suggesting the presence of an intermediate species distinct from either the equilibrium ~510 or ~490 cm^{-1} species.

Time-Resolved RR Spectra of H64L, H64V, H64A, and H64I. The TR^3 spectra of H64L are presented in Figure 5. The ν_{Fe-CO} band is completely absent for Δt_d = 0–20 ns but is definitely present for Δt_d = 100 ns. The original spectrum is almost restored at Δt_d = 100 μs, and the band center exhibits no shift during the recombination. Figure 6 shows the TR^3 spectra of H64V. Two ν_{Fe-CO} bands are present in the spectrum for Δt_d = −20 ns, and both bands disappear in the spectrum for Δt_d = 0 ns. If CO binds to the open form and is rapidly

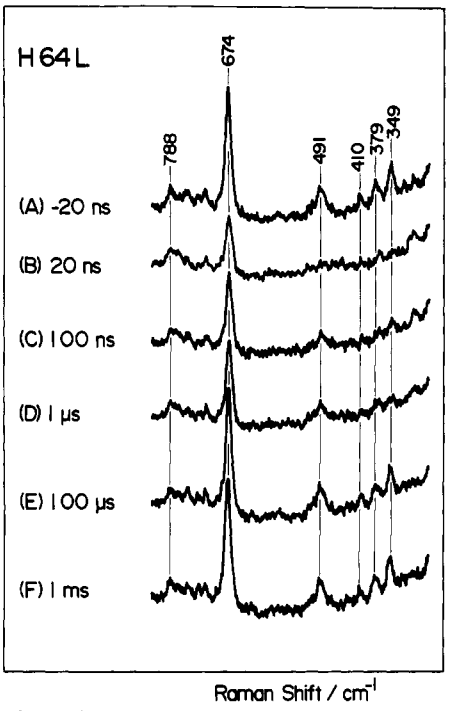

FIGURE 5: Pump/probe RR spectra in the ν_{Fe-CO} region of the E7-Leu mutant MbCO. Experimental conditions are the same as those for Figure 2.

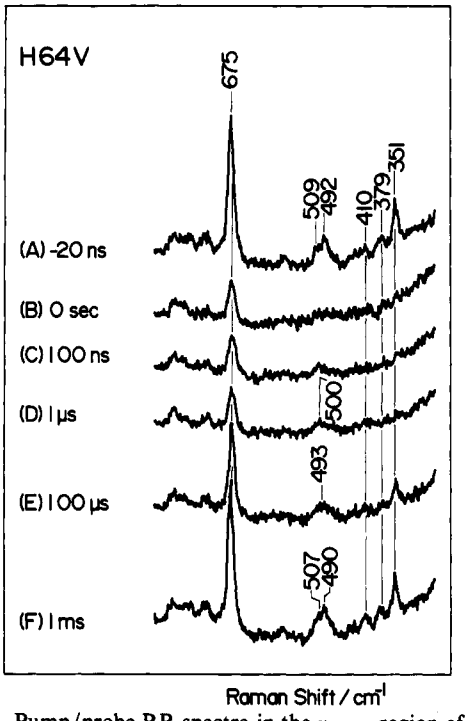

FIGURE 6: Pump/probe RR spectra in the ν_{Fe-CO} region of the E7-Val mutant MbCO. Experimental conditions are the same as those for Figure 2.

($<10^{-5}$ s) converted to the closed form, the TR^3 spectrum for Δt_d = 100 μs is expected to exhibit two bands at 509 and 492 cm^{-1} with the same relative intensity as that for Δt_d = −20 ns. In practice, a single broad band appeared between the two bands (~500 cm^{-1}) for Δt_d = 100 ns, and the band center gradually shifted to lower frequencies as Δt_d became longer. The two bands were not resolved in the spectra for Δt_d = 100 μs, as will be discussed later, but the original pattern was nearly restored for Δt_d = 1 ms.

The TR^3 spectra of H64A and H64I are shown in Figures 7 and 8, respectively. In the static spectra of these mutants

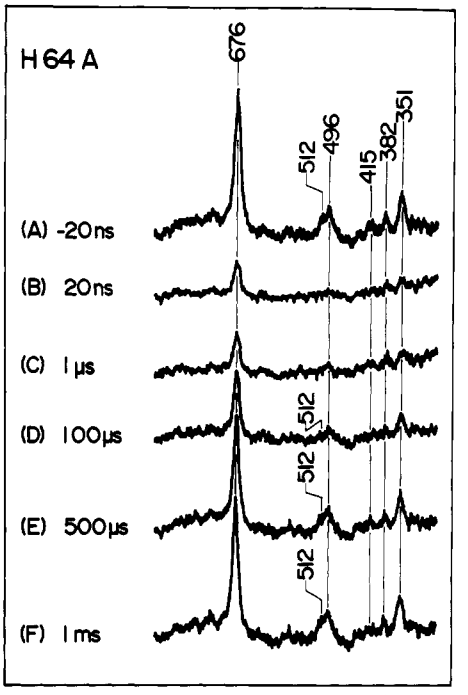

FIGURE 7: Pump/probe RR spectra in the ν_{Fe-CO} region of the E7-Ala mutant MbCO. Experimental conditions are the same as those for Figure 2.

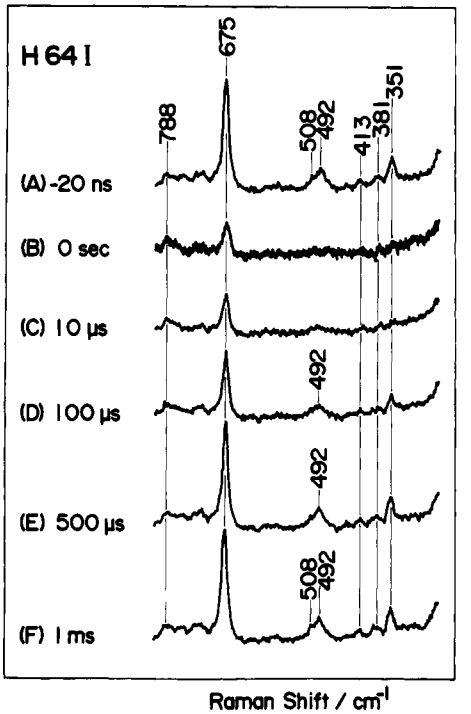

FIGURE 8: Pump/probe RR spectra in the ν_{Fe-CO} region of the E7-Ile mutant MbCO. Experimental conditions are the same as those for Figure 2.

(Δt_d = −20 ns), the presence of a side band at ~510 cm^{-1} besides the main band at 492–496 cm^{-1} is prominent. Both bands disappeared in the spectra for Δt_d = 0–20 ns. For H64A the low-frequency component is recognizable in the spectrum for Δt_d = 1 μs. The high-frequency component is discernible in the spectra for Δt_d > 100 μs. The relative intensity of the two bands appears to be restored after Δt_d = 500 μs. The corresponding two bands for H64I are not resolved in the spectrum for Δt_d = 10 μs, giving the appearance of a

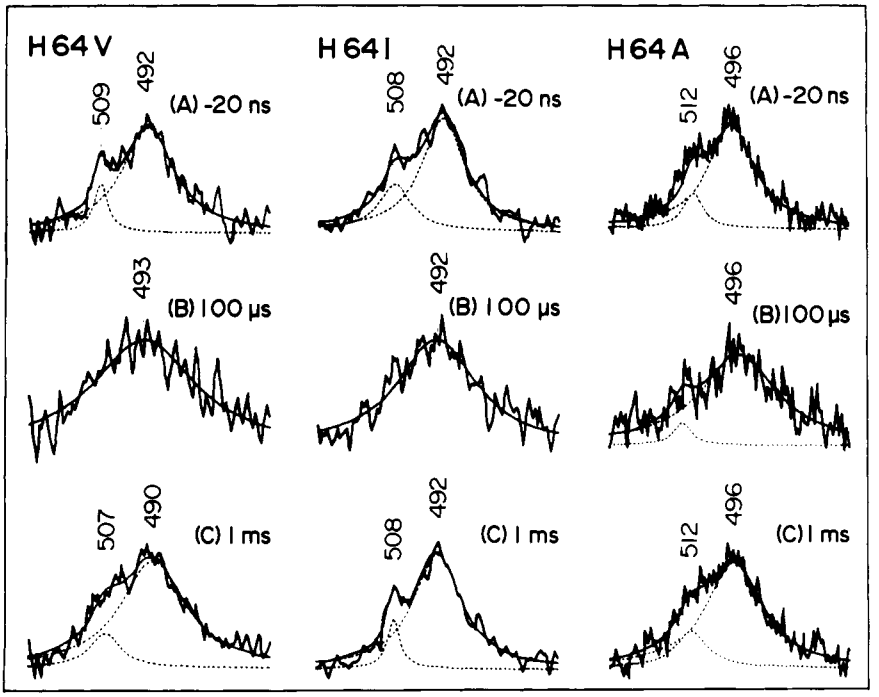

FIGURE 9: Band fitting calculations for the transient ν_{Fe-CO} bands of H64V, H64I, and H64A. The solid lines denote the sum of the calculated component spectra represented by broken lines: (A) Δt_d = −20 ns; (B) Δt_d = 100 μs; (C) Δt_d = 1 ms.

broad symmetric band at ~495 cm^{-1}, i.e., between the two static frequencies.

In order to investigate the temporal behavior of these ν_{Fe-CO} bands in more detail, the observed bands of H64V, H64I, and H64A were fit with two Lorentzian functions. Figure 9 illustrates the observed and calculated spectra of H64V, H64I, and H64A for Δt_d = −20 ns (A), 100 μs (B), and 1 ms (C). Since the S/N ratios of the observed spectra are not high enough, the component spectra deduced may contain significant errors. However, the peak frequencies of the component bands for the Δt_d = −20 ns spectra are in agreement with those for the Δt_d = 1 ms spectra for each of the species H64I and H64A. It is noted from this calculation that the spectra of H64V and H64I at Δt_d = 100 μs were reproduced with a single Lorentzian function but could not be uniquely fit by assuming the presence of two bands. It is only after 100 μs that the high-frequency component becomes recognizable. For H64A the spectrum for Δt_d = 100 μs was fit with two bands but is dominated by a band at 496 cm^{-1}.

Analysis of Data. A kinetic description of ligand binding to Mb has been proposed by Gibson et al. (1986). The most practical model is to assume two intermediate states between MbCO and Mb + CO, that is,

$$\text{MbCO} \leftrightarrow \text{contact pair} \leftrightarrow \text{protein-separated pair} \leftrightarrow \text{deoxyMb} + \text{CO} \quad (1)$$

In earlier days, the bimolecular rebinding of photodissociated CO to deoxyMb was treated using a single exponential function (Henry et al., 1983), but the present results could not be reproduced with such a model despite there being no inhomogeneity present in the sample, as described in the Experimental Procedures. This was also true with horse MbCO at pH 8.0 (Sakan et al., 1992). Therefore, it was assumed that the recovery of MbCO followed a biexponential growth, that is,

$$[\text{MbCO}] = A_1\{1 - \exp(-k_1 t)\} + A_2\{1 - \exp(-k_2 t)\} \quad (2)$$

The phenomenological parameters can be related to the rate constants of the individual elementary processes of eq 1 under specified conditions (Gibson et al., 1986). The recombination from the contact pair is called the geminate process and reflects the rate of bond formation, which has been determined as 10^9 s^{-1} (Traylor et al., 1992). Recently, the geminate recombination has been represented by a stretched exponential or biexponential function (Tian et al., 1992). Since the flash photolysis experiments by Eaton and co-workers (Henry et al., 1983) indicated that the geminate rebinding occurs with a relaxation time of 180 ns and its contribution over the first 180 ns is less than 4% of the total for MbCO, it does not contribute significantly to the spectra observed in this study. Here, for the sake of convenience, we describe the k_1 and k_2 processes as the fast and slow phases, respectively, which are approximately composed of the recombination of a protein-separated pair and the bimolecular reaction, respectively.

The integrated intensities of the ν_{Fe-CO} bands have been determined for all spectra. When a given band consisted of two components, their sum was taken as the integrated intensity. Relative values with regard to the intensity at Δt_d = −20 ns for each species are plotted against the delay time in Figures 10 and 11. The broken lines represent the values calculated with eq 2 and the parameters listed in Table I. Note that these rate constants correspond to the values for a CO pressure of 1 atm.

Figure 10 contains the plots for H64H, H64G, and H64Q. All of them have the equilibrium ν_{Fe-CO} band in the frequency region of the closed form, but their recovery behaviors differ. H64H and H64G have similar fast phases whose rate constants are ~2 × 10^4 s^{-1} which dominate over the first 30% of the recovery, but their slow phases are different; a larger k_2 for H64G leads to a faster recovery at 1 ms. H64Q exhibits a rate of recovery 5 times faster than that of H64H for the fast phase, while their slow phases are alike.

Figure 11 plots the results of H64L, H64V, H64I, and H64A. H64I and H64A (Figure 11A) involve a dominant fast phase over the first 20% of recovery, and their rate

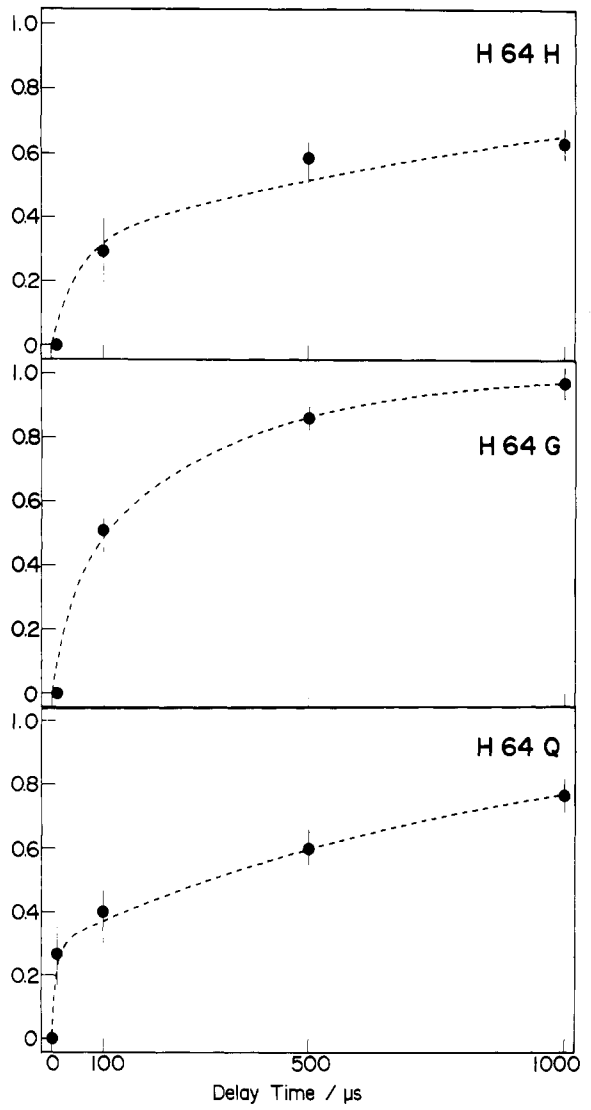

FIGURE 10: Recovery of the CO-bound forms for H64H, H64G, and H64Q. Experimental points represent the relative area intensity at each Δt_d value with regard to that for $\Delta t_d = -20$ ns. The broken lines denote the values calculated from eq 2 and parameters listed in Table I.

Table I: Rebinding Rate Constants and Amplitudes of Photodissociated MbCO's[a]

	k_1/s^{-1}	k_2/s^{-1}	A_1	A_2
H64H	2.0×10^4	6.9×10^2	0.31	0.69
H64G	2.5×10^4	3.2×10^3	0.33	0.67
H64Q	1.0×10^5	1.1×10^3	0.29	0.71
H64L	5.5×10^6	2.5×10^4	0.83	0.17
H64V	2.5×10^6	3.1×10^3	0.50	0.50
H64I	2.0×10^5	1.2×10^4	0.17	0.83
H64A	3.0×10^5	3.2×10^3	0.23	0.77

[a] These values were estimated by a trial and error method for curve fitting with eq 2.

constants are ~10 times larger than that of H64H. H64I is different from H64A with regard to the slow phase. In contrast, H64L and H64V (Figure 11B) have much larger contributions from the fast phase, and their rate constants are 100–200 times larger than that of H64H, while the rate of the slow phase of H64V is similar to those of H64A and H64G. The faster rebinding of CO in H64L compared with that in H64H is qualitatively (but not quantitatively) in agreement with the results of Carver et al. (1990), who reported that for sperm whale MbCO the kinetic parameter for rebinding from the protein-separated pair is 20 times faster for H64L than for H64H and that the rate of entry to the protein is also 6 times faster (k_1 and k_2 of H64L are 270 and 40 times larger than those of H64H, respectively).

DISCUSSION

Controlling Factors of the CO Recombination. The present experiments demonstrated that MbCO whose ν_{Fe-CO} is 490–495 cm^{-1} recovers from photodissociation much faster than those species whose ν_{Fe-CO} values are 505–510 cm^{-1}. Therefore, a factor which determines the static ν_{Fe-CO} frequency is essential to a discussion of the kinetics of the CO recombination. To date, the species with ν_{Fe-CO} at 490–495 and 505–510 cm^{-1} have been thought to have the upright and distorted structures, respectively, on the basis of the following observations: the protein-free heme–CO complex with imidazole as a trans ligand, which has an upright geometry (Peng & Ibers, 1976), gives the ν_{Fe-CO} band at 495 cm^{-1} in organic solution (Evangelista-Kirkup et al., 1986), while the CO–heme with an intermediate length of strap, in which the upright geometry is sterically prohibited, gives the ν_{Fe-CO} band at 506 cm^{-1} in organic solution (Yu et al., 1983). The distorted structure in native MbCO is considered to be a consequence of steric hindrance of His-64 (E7) (Collman et al., 1983). However, the results shown in Figure 1 demonstrate that the steric hindrance from the E7 residue is not the main factor for the determination of the ν_{Fe-CO} frequency, as pointed out by Nagai et al. (1987), since a small group, E7-Gly, gives ν_{Fe-CO} at 504 cm^{-1} while a bulky group, E7-Ile, gives ν_{Fe-CO} at 492 cm^{-1}. As far as the frequencies of the main ν_{Fe-CO} bands in Figure 1 are concerned, polar and nonpolar residues at E7 seem to give rise to ν_{Fe-CO} values at 505–510 and 490–495 cm^{-1}, respectively.

A relation between the ν_{Fe-CO} frequency and the Fe–C–O valence angle or tilting of the Fe–C bond has been investigated theoretically (Yu et al., 1983; Yu et al., 1988; Li & Spiro, 1988; Nagai et al., 1991), and some models have been proposed. In these treatments, a set of potential constants, which can reproduce the observed frequencies for the equilibrium state, is used to predict the frequencies expected for other geometries. Unfortunately, the models are not complementary; one calculation predicts that the ν_{Fe-CO} frequency becomes lower as the Fe–C–O bending angle becomes smaller (Li & Spiro, 1988), but the other predicts the opposite (Nagai et al., 1991). This discrepancy arises from the different assignments of the Fe–C–O bending RR band (Tsuboi, 1988); the observed Fe–C–O bending RR band around 580 cm^{-1} was assumed to be a fundamental in the former (Li & Spiro, 1988) but an overtone in the latter (Nagai et al., 1991), and in the former the stretching–bending interaction determines the frequency while in the latter only the kinetic coupling influences the frequency. Another serious problem in these theoretical treatments is the use of the same force constants for different geometrical structures.

Oldfield and co-workers (Augspurger et al., 1991) pointed out that the ν_{CO} frequency is also affected by the electronic polarization of the CO bond and, thus, in the protein by the electric field at CO generated by surrounding amino acid residues. On the basis of this idea, CO would be more polarized when the E7 residue is more polar. Generally, polar residues are more hydrophilic. Accordingly, we adopted a parameter representing the hydrophilic character of the E7 residue, that is, the hydropathy index (Kyte & Doolittle, 1982). The static ν_{Fe-CO} frequencies shown in Figure 1 are plotted against the hydropathy index of the substituted E7 residue in Figure 12.

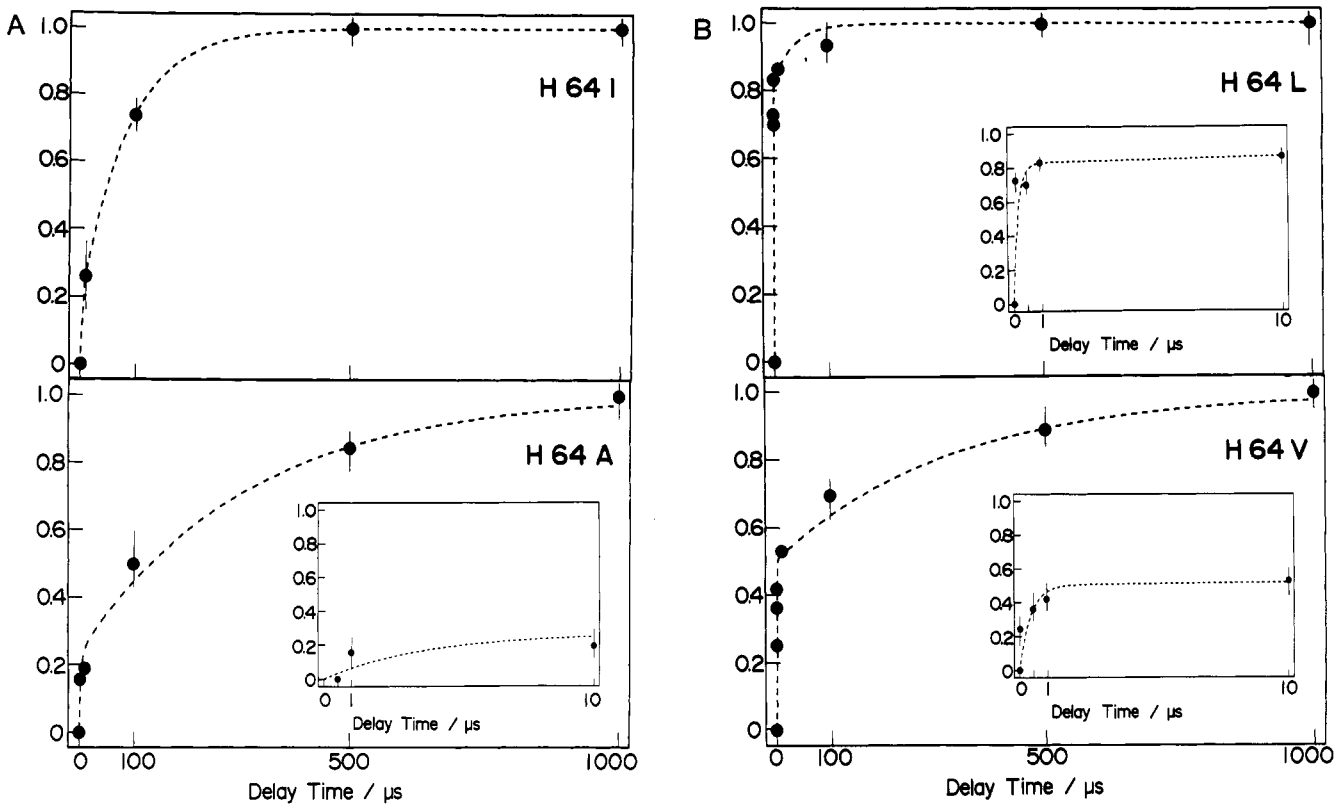

FIGURE 11: Recovery of the CO-bound forms of H64I and H64A (A) and H64L and H64V (B). The insertions represent the expanded versions of the same curves for the shorter Δt_d region. Experimental points and broken lines as for Figure 10.

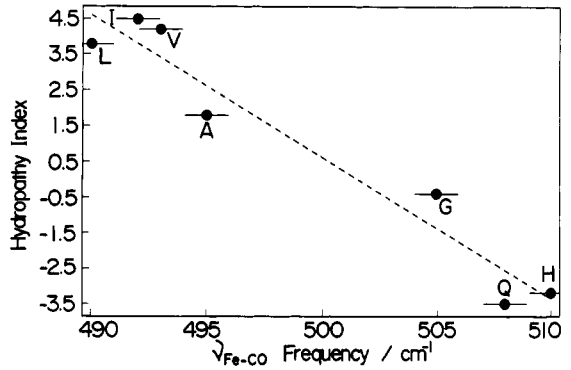

FIGURE 12: Relation between the observed ν_{Fe-CO} frequencies and the hydropathy index of the E7 residue. The values of the hydropathy index for individual amino acids were taken from Kyte and Doolittle (1982).

A good linear correlation is found, and it is empirically evident that the ν_{Fe-CO} frequency becomes lower as the environment around CO becomes more hydrophobic. This may suggest that the surrounding electric field effect causes some change simply in the CO bond polarization without altering the geometry of heme–CO or causing structural changes in Lys-45 and nearby residues which influence the geometrical structure of the Fe–C–O unit.

When this polarization model is correct, the words, open and closed, might be misleading, since the closed form also allows CO to enter into the heme pocket without going by way of the open form, although multiple conformations are postulated with the polarization model. Here, one would ask why CO binds faster for more hydrophobic environments. There is no definite answer for this, but as one of the plausible interpretations, we note that the solubility of CO is significantly higher for hydrophobic than hydrophilic solvents: 0.029 (0.021) mL/mL for H_2O and 0.170 (0.184) mL/mL for benzene at 10 °C (25 °C), which indicates stabilization of CO by ΔG = 5.4 kJ/mol more in benzene than in water. In other words, the photodissociated CO is more stabilized when the heme pocket is more hydrophobic.

This conclusion would yield some difference in the potential minimum corresponding to the protein-separated pair of eq 1, as illustrated in Figure 13. The lower free energy for it with the hydrophobic heme pocket would raise the probability that CO became trapped in this potential minimum rather than escaped into the solvent after photodissociation. Accordingly, it is qualitatively understandable that the more hydrophobic heme pocket results in faster recombination (Rohlfs et al., 1990; Carver et al., 1990) as well as the lower ν_{Fe-CO} frequency. In this case, interpretation for the presence of two ν_{Fe-CO} bands in a single species is somewhat difficult; we have to assume the presence of two protein conformations, particularly for distal residues which yield different polarization effects on the CO bound to the heme.

According to the X-ray crystallographic analysis on sperm whale MbO_2 (Phillips, 1980), a hydrogen bond is formed between E7-His (His-64) and CD3-Arg (Arg-45) via a water molecule, as illustrated in Figure 14. Kuriyan et al. (1986) pointed out that the side chain of the CD3-Arg of sperm whale MbCO stays in two equally populated conformations and that one of the two structures allows the entry of CO into the binding site, since it does not block the motion of the distal His out of the heme pocket. For human Mb, on the other hand, the CD3 residue is replaced by Lys. The replacement of the CD3 residue (Lys-45) with Arg for human Mb (K45R) has yielded a faster bimolecular recombination rate of CO (Lambright et al., 1989). Although there is no X-ray analysis for wild-type human Mb, the CD3 Lys is deduced to interact with E7-His. Such interactions would be facilitated when the E7 residue is hydrophilic, similar to the CD3 residue.

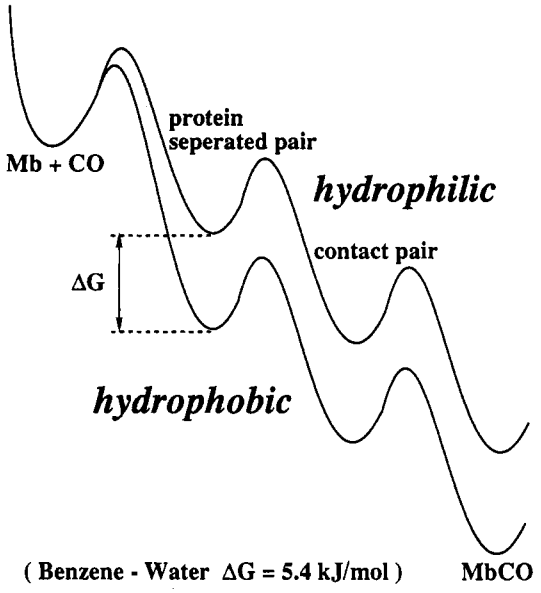

FIGURE 13: Schematic energy diagram for binding of CO to Mb. Contact pair means the state in which the Fe–CO bond is cleaved in the bound geometry of CO, and protein-separated pair implies that CO is somewhere in the protein. The potential minimum for the protein-separated pair is thought to be lower for a hydrophobic than for a hydrophilic E7 residue, although other parts are regarded to be the same in this approximation. The energy difference deduced from the solubility of CO in water and benzene is 5.4 kJ/mol, but the actual difference for MbCO between hydrophilic and hydrophobic E7 residues would be much smaller than this value.

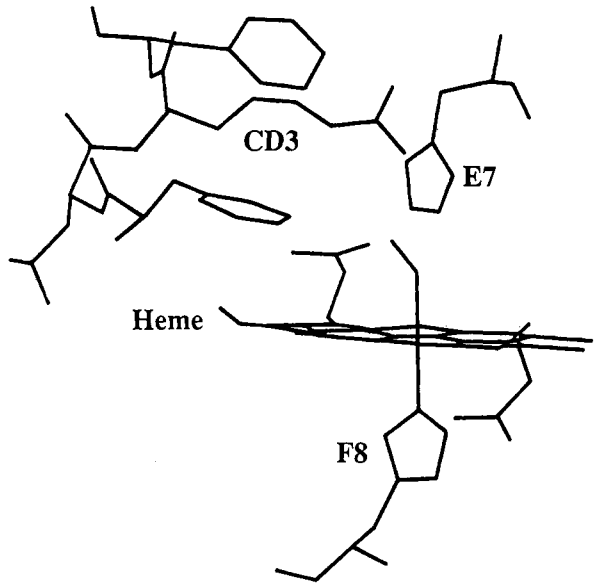

FIGURE 14: Structure of the heme pocket of MbCO reproduced from Kuriyan et al. (1986). The CD3 residue is Arg-45 for sperm whale Mb and Lys-45 for human Mb.

As a measure of the ease of their interaction, the relative hydropathy values (χ) of CD3 Lys and E7-His might serve as a parameter. In this idea, as the difference, $\chi_{E7} - \chi_{CD3}$, becomes larger, the two residues would repel each other. This corresponds to a measure of the hydrophobicity of the E7 residue relative to that of the CD3 residue. If this idea is accepted, it is possible to interpret qualitatively the difference in the ν_{Fe-CO} frequencies of the Gly-64 mutant of human MbCO (505 cm^{-1}, Figure 1) and sperm whale MbCO (492 cm^{-1}) (Morikis et al., 1989) and also that of the wild-type human MbCO (510 cm^{-1}, Figure 1) and sperm whale MbCO (508 cm^{-1}) (Morikis et al., 1989). The CD3 residue of sperm whale Mb is Arg with $\chi = -4.5$, but that of human Mb is Lys with $\chi = -3.8$ (negative values meaning hydrophilic residues). $\chi_{E7} - \chi_{CD3}$ is positively shifted with sperm whale Mb, and the ν_{Fe-CO} frequency is therefore expected to be lower for sperm whale Mb than for human Mb.

Recombination Dynamics. The photodissociation of MbCO is characterized by a high quantum yield (nearly unity) in contrast with other cases (0.13 for MbO_2 and much smaller for MbNO) (Gibson et al., 1986). This implies that the escape from the contact pair valley in Figure 13 is the largest for CO among small ligands. On the other hand, the rate-limiting step for binding of CO is reported to be the bond formation step, in contrast with that of O_2 for which the rate-limiting step is the ligand entry (Gibson et al., 1986; Adachi & Morishima, 1989).

The present results suggest that CO binding to Mb takes place in two phases, but their rate constants cannot be systematically grouped into two. In the case of H64H, the reference species, the ν_{Fe-CO} band exhibited no frequency shift, and throughout the recombination process there was no transient band discernible around 490 cm^{-1}. For H64G, a transient band was recognizable around 100 μs. Since the interaction time between a molecule and a photon is sufficiently short, two bands corresponding to the open and closed forms should appear without exhibiting a frequency shift when there is interconversion between the two forms, which occurs presumably on the order of 100 μs. This transient band is significantly broader but its band center is not greatly different from the equilibrium one. Thus, it suggests the presence of slight structural disorder of the distal residues (or an appreciable distribution of the heme–CO bent angles) in the bond formation process. If the structure with ν_{Fe-CO} at $\sim$490 cm^{-1} is a precursor of the closed form, the corresponding band should have appeared in the specta of H64H, H64G, and H64Q for Δt_d = 100 ns to 10 μs. Its absence strongly suggests that CO entry goes by way of a protein rearrangement which is distinct from an open structure intermediate, i.e., the swinging out of the His-64 side chain.

H64L and H64V have noticeably large rate constants for the fast phase and their amplitudes are large. H64L always exhibits the ν_{Fe-CO} band at the equilibrium position (491 cm^{-1}), although the bandwidth is somewhat broader for Δt_d = 100–1000 ns. H64V consists of two bands (509 and 492 cm^{-1}), but the earlier transient species gives a broad feature at the frequency between the two bands, and afterward its band center approaches the frequency of the low-frequency component. It is likely that the fast component corresponds to recombination from the minimum of the protein-separated pair, which is deeper for the hydrophobic E7 residues than for hydrophilic E7 residues, and that the frequency shift reflects slight structural relaxation of the distal residues.

H64I and H64A have similar rate constants for the fast phase, although its dominance only spans the first 20% of the recovery for these Mb. Both have two ν_{Fe-CO} bands in the equilibrium state, but the frequency of the transient band around 1–100 μs is nearly equal to that of its low-frequency counterpart. The high-frequency counterpart contributes only after 100 μs. If the interconversion between the open and closed forms is sufficiently fast, the equilibrium intensity ratio of the high- and low-frequency components should be attained earlier, but it was attained at 500–1000 μs.

In conclusion, we found that MbCO with ν_{Fe-CO} around $\sim$510 cm^{-1} is not generated via a $\sim$490 cm^{-1} (open) precursor. It is evident that there are two protein conformations corresponding to ν_{Fe-CO} = 492–496 cm^{-1} and ν_{Fe-CO} = 508–

512 cm^{-1}, of which the former binds CO significantly faster than the latter, and that the two conformations are not interconverted within 100 μs. Since the ν_{Fe-CO} frequencies seem to depend on the hydrophobicity of the E7 residue, and the photodissociated CO is stabilized more in hydrophobic than in hydrophilic environments, it is likely that the hydrophobicity of the heme pocket and the conformation of a few distal residues are significant for the determination of the CO recombination rate.

ACKNOWLEDGMENT

The authors thank Dr. S. G. Boxer and Mr. S. Balasubramanian for the human Mb expression system and suggestions, Dr. S. Kimura for oligonucleotide synthesis, Miss D. A. Shelley and Miss E. J. McKelvey for assistance, and Dr. P. J. Jewsbury for reading this manuscript.

REFERENCES

Abe, M., Kitagawa, T., & Kyogoku, Y. (1978) *J. Chem. Phys. 69*, 4526–4534.
Adachi, S., & Morishima, I. (1989) *J. Biol. Chem. 264*, 18896–18901.
Anfinrud, P. A., Han, C., & Hochstrasser, R. M. (1989) *Proc. Natl. Acad. Sci. U.S.A. 86*, 8387–8391.
Augspurger, J. D., Dykstra, C. E., & Oldfield, E. (1991) *J. Am. Chem. Soc. 113*, 2447–2451.
Braunstein, D., Ansari, A., Berendzen, J., Cowen, B. R., Egeberg, K. D., Frauenfelder, H., Hong, M. K., Ormos, P., Sauke, T. B., Scholl, R., Schulte, A., Sligar, S. G., Springer, B. A., Steinbach, P. J., & Yound, R. D. (1988) *Proc. Natl. Acad. Sci. U.S.A. 85*, 8497–8501.
Carver, T. E., Rohlfs, R. J., Olson, J. S., Gibson, Q. H., Blackmore, R. S., Springer, B. A., & Sligar, S. G. (1990) *J. Biol. Chem. 265*, 20007–20020.
Collman, J. P., Brauman, J. I., Iverson, B. L., Sessler, J. L., Morris, R. M., & Gibson, Q. H. (1983) *J. Am. Chem. Soc. 105*, 3052–3064.
Evangelista-Kirkup, R., Smulevich, G., & Spiro, T. G. (1986) *Biochemistry 25*, 4420–4425.
Gibson, Q. H., Olson, J. S., McKinnie, R. E., & Rohlfs, R. J. (1986) *J. Biol. Chem. 261*, 10228–10239.
Han, S., Rousseau, D. L., Giacometti, G., & Brunori, M. (1990) *Proc. Natl. Acad. Sci. U.S.A. 87*, 205–209.
Henry, E. R., Sommer, J. H., Hofrichter, J., & Eaton, W. A. (1983) *J. Mol. Biol. 166*, 443–451.
Hofrichter, J., Sommer, J. H., Henry, E. R., & Eaton, W. A. (1983) *Proc. Natl. Acad. Sci. U.S.A. 80*, 2235–2239.
Ikeda-Saito, M., Lutz, R. S., Shelley, D. A., McKelvey, E. J., Mattera, R., & Hori, H. (1991) *J. Biol. Chem. 266*, 23641–23647.
Johnson, K. A., Olson, J. S., & Phillips, G. N., Jr. (1989) *J. Mol. Biol. 207*, 459–463.
Kitagawa, T. (1986) *Spectroscopy of Biological Systems* (Clark, R. J. H., Hester, R. E., Eds.) pp 443–481, Wiley (Heyden), Chichester, UK.
Kitagawa, T., Ondrias, M. R., Rousseau, D. L., Ikeda-Saito, M., & Yonetani, T. (1982) *Nature 298*, 869–871.
Kuriyan, J., Wilz, S., Karplus, M., & Petsko, G. A. (1986) *J. Mol. Biol. 192*, 133–154.
Kyte, J., & Doolittle, R. F. (1982) *J. Mol. Biol. 157*, 105–132.
Lambright, D. G., Balasubramanian, S., & Boxer, S. G. (1989) *J. Mol. Biol. 207*, 289–299.
Levenberg, K. Q. (1944) *Appl. Math. 2*, 164.
Li, X.-Y., & Spiro, T. G. (1988) *J. Am. Chem. Soc. 110*, 6024–6033.
Lin, S.-H., Yu, N.-T., Tame, J., Shih, D., Renaud, J.-P., Pagnier, J., & Nagai, K. (1990) *Biochemistry 29*, 5562–5566.
Martin, J. L., Migus, A., Poyart, C., Lecarpentier, Y., Astier, R., & Antonetti, A. (1983) *Proc. Natl. Acad. Sci. U.S.A. 80*, 173–177.
Moore, J. N., Hansen, P. A., & Hochstrasser, R. M. (1988) *Proc. Natl. Acad. Sci. U.S.A. 85*, 5062–5066.
Morikis, D., Champion, P. M., Springer, B. A., & Sligar, S. G. (1989) *Biochemistry 28*, 4791–4800.
Nagai, K., Luisi, B., Shih, D., Miyazaki, G., Imai, K., Poyart, C., DeYoung, C., Kwiatkowsky, L., Noble, R. W., Lin, S.-H., & Yu, N.-T. (1987) *Nature (London) 329*, 858–860.
Nagai, M., Yoneyama, Y., & Kitagawa, T. (1991) *Biochemistry 30*, 6495–6503.
Patrich, J. W., Poyart, C., & Martin, J. L. (1988) *Biochemistry 27*, 4049–4060.
Peng, S.-M., & Ibers, J. A. (1976) *J. Am. Chem. Soc. 98*, 8032–8036.
Phillips, S. E. V. (1980) *J. Mol. Biol. 142*, 531–554.
Phillips, S. E. V., & Shoenborn, B. P. (1981) *Nature 292*, 81–82.
Ramsden, J., & Spiro, T. G. (1989) *Biochemistry 28*, 3125–3128.
Rohlfs, R. J., Mathews, A. J., Carver, T. E., Olson, J. S., Springer, B. A., Egeberg, K. D., & Sligar, S. G. (1990) *J. Biol. Chem. 265*, 3168–3176.
Sage, J. T., Morikis, D., & Champion, P. M. (1991) *Biochemistry 30*, 1227–1237.
Sakan, Y., Ogura, T., & Kitagawa, T. (1992) *Chem. Phys. Lett. 196*, 150–154.
Senga, Y., & Minami, S. (1986) *Bunko Kenkyu 33*, 92–101.
Spiro, T. G., Ed. (1989) *Biological Applications of Raman Spectroscopy*, Vol. 3, Wiley-Interscience, New York.
Srajer, V., Reinisch, L., & Champion, P. M. (1991) *Biochemistry 30*, 4886–4895.
Tian, W. D., Sage, J. T., Srajer, V., & Champion, P. M. (1992) *Phys. Rev. Lett. 68*, 408–411.
Traylor, T. G., Magde, D., Taube, D. J., Jongeward, K. A., Bandyopadhyay, D., Luo, J., & Walda, K. N. (1992) *J. Am. Chem. Soc. 114*, 417–429.
Tsubaki, M., Srivastava, R. B., & Yu, N. T. (1982) *Biochemistry 21*, 1132–1140.
Tsuboi, M. (1988) *Indian J. Pure Appl. Phys. 26*, 188–191.
Varadarajan, R., Szabo, A., & Boxer, S. G. (1985) *Proc. Natl. Acad. Sci. U.S.A. 82*, 5681–5684.
Varadarajan, R., Lambright, D. G., & Boxer, S. G. (1989) *Biochemistry 28*, 3771–3781.
Yonetani, T., Yamamoto, H., & Iizuka, T. (1974) *J. Biol. Chem. 249*, 2168–2174.
Yu, N. T., & Kerr, E. A. (1988) in *Biological Applications of Raman Spectroscopy* (Spiro, T. G., Ed.) Vol. 3, pp 40–95, Wiley-Interscience, New York.
Yu, N. T., Kerr, E. A., Ward, B., & Chang, C. K. (1983) *Biochemistry 22*, 4534–4540.
Zhu, L., Sage, J. T., Rigos, A. A., Morikis, D., & Champion, P. M. (1992) *J. Mol. Biol. 224*, 207–215.